Novel Microwave Network for the Leaky-Wave Analysis of Evanescent Fields in Stub-Loaded Structures

José Luis Gómez-Tornero, *Member, IEEE*, Fernando Daniel Quesada-Pereira, *Member, IEEE*, and Alejandro Álvarez-Melcón, *Senior Member, IEEE*

***Abstract*—In this paper, a new transverse equivalent network for the modal analysis of stub-loaded leaky-wave antennas is developed. The derived network is useful for the study of the radiation of evanescent fields that occurs when they reach the top aperture of the parallel-plate stub. This transverse network is based, for the first time, on a nonhybrid formulation of the constituent parallel-plates modes of order 1 (TE_1^Z and TM_1^Z). The obtained network is an alternative to the one based on hybrid TE_1^Y and TM_1^Y modes, and leads to a simpler transverse resonance equation. The new equivalent network is validated by obtaining leaky-mode dispersion curves for a previously studied leaky-wave antenna in nonradiative dielectric guide technology.**

***Index Terms*—Nonradiative dielectric (NRD) leaky-wave antennas, stub-loaded leaky-wave antennas, transverse equivalent circuit.**

I. Introduction

LEAKY-WAVE antennas loaded with parallel plates (also known as stub-loaded leaky-wave antennas) have been widely studied for many applications [1]–[7]. Some examples of stub-loaded leaky-wave antennas are shown in Fig. 1. The parallel plates, of height L and separated a distance a, act as a filtering mechanism, which interconnects a waveguide and the top radiating aperture. The fields in the parallel-plates region can be expanded as a sum of parallel-plate modes. The parallel plates, separated a distance $a < \lambda_0/2$ (where λ_0 is the free-space wavenumber), allow only the main parallel-plate mode (TE_0) to propagate along the z-direction (see reference axis in Fig. 1). Higher order parallel-plate modes are below cutoff in the z-direction, therefore having an exponential-decaying evanescent behavior as they propagate through the stub-region [4]. If the height L is large enough, higher order parallel-plate modes will not reach the radiating top aperture and their contribution to radiation can be neglected [1]–[4].

Manuscript received September 17, 2007; revised March 4, 2008. This work was supported under the Spanish National Project TEC2004-04313-C02-02/TCM, under the Regional Seneca Project 02972/PI/05, and under Regional Scholarship PMPDI-UPCT-2007.

The authors are with the Department of Communication and Information Technologies, Technical University of Cartagena, Cartagena 30202, Spain (e-mail: josel.gomez@upct.es; fernando.quesada@upct.es; alejandro.alvarez@upct.es).

Color versions of one or more of the figures in this paper are available online at http://ieeexplore.ieee.org.

Digital Object Identifier 10.1109/TMTT.2008.923880

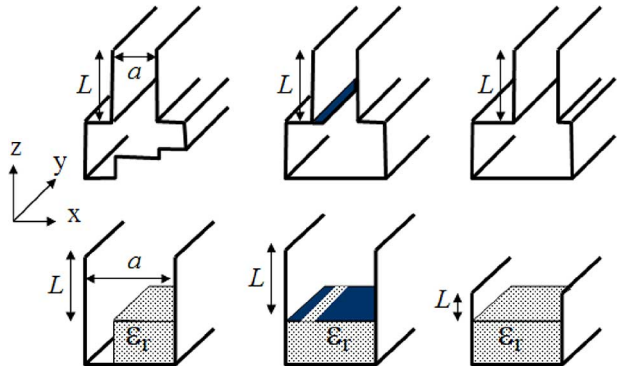

Fig. 1. Different stub-loaded leaky-wave antennas.

On the other hand, the radiation of the first higher order parallel-plate modes (TE_1 and TM_1) has also been used for the case of the nonradiative dielectric (NRD) leaky-wave antenna [8]–[11]. In this case, the stub height L is shortened to allow these higher order parallel-plate modes to reach the top radiating aperture, and to induce radiation, as illustrated in the antenna shown in the bottom-right area of Fig. 1. In any case, the analysis of these leaky-wave antennas can be simplified by developing an equivalent transverse network in which the radiating impedance that models the top aperture plays a fundamental role. The equivalent radiation impedance depends on the parallel-plate mode, which reaches the top aperture and contributes to radiation. For the case of radiation of the main parallel-plate mode (TE_0) in stub-loaded leaky-wave antennas, Marcuvitz's radiation impedance [12] has been extensively used in many equivalent circuits [1]–[7]. For the case of the stub-shortened NRD leaky-wave antenna, a novel equivalent radiation impedance was developed by Sanchez and Oliner to model the radiation of the evanescent first higher order parallel-plate modes (TE_1 and TM_1, which are below cutoff) [9], [10]. The equivalent transverse network developed in [10] for the leaky-mode analysis of the stub-shortened NRD leaky-wave antenna is illustrated in Fig. 2(a).

As explained in detail in [10], one can choose two different sets of vector modal functions to describe these first higher order parallel-plate modes, namely, the TE_1^Z and TM_1^Z set or the TE_1^Y and TM_1^Y set. The first election corresponds to the ordinary set of parallel-plate modes (TE_1^Z and TM_1^Z) in which the propagation direction of the transverse equivalent transmission line (z-axis, see Fig. 2) is the same as the propagation direction used in the transverse-longitudinal formulation of the modes.

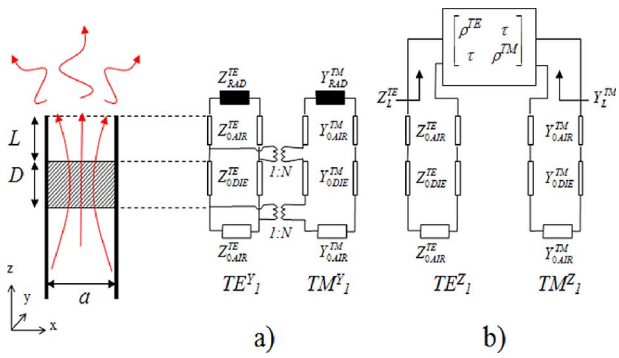

Fig. 2. Equivalent transverse networks to model leaky-wave antenna. (a) Hybrid model developed in [10]. (b) Nonhybrid model proposed in this study.

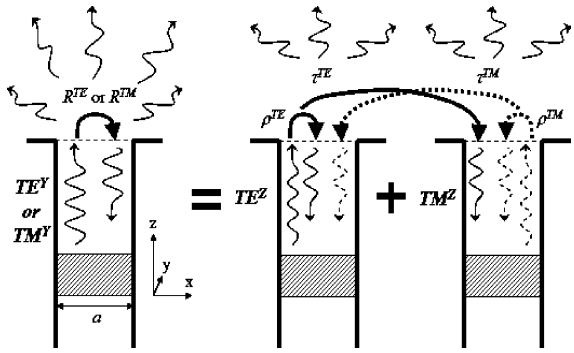

Fig. 3. TE^Y or TM^Y parallel-plate mode incident at radiating open end.

On the contrary, the second set (TE_1^Y and TM_1^Y) corresponds to hybrid longitudinal section magnetic (LSM) and longitudinal section electric (LSE) modes, which are defined with respect to the y-axis, transverse to the z-direction of propagation of the equivalent transmission lines. If ordinary TE_1^Z and TM_1^Z modes are employed, the air–dielectric interfaces will be represented as simple junctions between equivalent transmission lines, as can be seen in Fig. 2(b) (the modes do not couple in the air–dielectric interface). However, these modes become coupled by the top radiating discontinuity. Therefore, equivalent reflection coefficients for each TE_1^Z and TM_1^Z parallel-plate mode do not independently exist. On the contrary, hybrid TE_1^Y and TM_1^Y parallel-plate modes remain uncoupled in the radiating aperture. In this case, it is possible to compute an equivalent terminal impedance to model the radiating open end, separately for TE_1^Y and TM_1^Y modes. These impedances are represented in Fig. 2(a) as $Z_{\mathrm{RAD}}^{\mathrm{TE}}$ and $Y_{\mathrm{RAD}}^{\mathrm{TM}}$. The equivalent reflection coefficients for the TE_1^Y and TM_1^Y parallel-plate modes were derived in [10] from the results of Weinstein [13], which were extended for the case of modes below cutoff with oblique incidence. Therefore, the use of hybrid parallel-plate modes simplifies the model of the radiating open end of the parallel plates if compared to the use of ordinary TE_1^Z and TM_1^Z parallel-plate modes. However, the model for the air–dielectric interface is more complicated for hybrid modes since one has to take into account the coupling between TE_1^Y and TM_1^Y. As can be seen in Fig. 2(a), the coupling was modeled in [10] using equivalent transformers in the air–dielectric interfaces. This coupling complicates the derivation of the transverse resonance equation, which is needed to find the permitted modes of the structure.

In this study, a completely original transverse network [shown in Fig. 2(b)] has been developed using ordinary TE_1^Z and TM_1^Z parallel-plate modes. Simple transmission lines connections are used for air–dielectric interfaces. Since these modes are coupled at the radiating open end, a two-port circuit represented by its four constituent S-parameters is used to model the radiation impedance and the coupling due to the top radiating aperture, as is illustrated in Fig. 2(b). This original two-port circuit is derived using an indirect approach. The idea is to derive the reflection and coupling coefficients of the TE_1^Z and TM_1^Z parallel-plate modes from the known reflection coefficients of the hybrid TE_1^Y and TM_1^Y modes [10]. Once the equivalent circuit is developed in Section II, results for a previously studied NRD leaky-wave antenna [9], [10] are presented in Section III to validate this original, simple, and accurate theory. The main contribution of this new model is the simple and analytical derivation of the transverse resonance equation, which is needed to compute the leaky-mode dispersion curves.

II. Development of Transverse Equivalent Network for TE^Z and TM^Z Modes

Fig. 3 represents a situation in which a TE_1^Y or a TM_1^Y parallel-plate wave propagates along the parallel plates, and it is incident at the top radiating aperture, part of the energy being radiated, and the rest of the energy being reflected back to the parallel-plate waveguide. As was mentioned before, hybrid TE_1^Y and TM_1^Y modes do not couple due to the radiating open end, and a simple reflection coefficient (R^{TE} or R^{TM}) can be used to model the top discontinuity [10]. Let us first analyze the case in which a TE_1^Y parallel-plate mode is incident at the radiating discontinuity, modeled with R^{TE}. The TE_1^Y field can be decomposed into the sum of a TE_1^Z and a TM_1^Z mode since they form an algebraic set of vector-basis functions. The TE_1^Z and TM_1^Z parallel-plate modes suffer a reflection at the top radiating discontinuity (modeled with ρ^{TE} and ρ^{TM}), but also a coupling between them. This coupling makes the incident TE_1^Z mode to induce a TM_1^Z mode (modeled with τ^{TE}), and in the same manner, the TM_1^Z mode creates a TE_1^Z mode (modeled with τ^{TM}). The energy carried by each TE_1^Z or TM_1^Z wave, which is not reflected or coupled, is transformed into radiation. This situation is sketched in Fig. 3, where all the associated reflection and coupling coefficients are illustratively represented.

As sketched in Fig. 3, the total electric field in this scenario can be expressed as a TE_1^Y field or, consistently, as a sum of a TE_1^Z wave and a TM_1^Z wave, each one with a given complex factor (A and B, respectively). This projection of the TE_1^Y wave in the TE_1^Z and TM_1^Z algebraic basis is, therefore, expressed as

$$\vec{E} = \vec{E}_{\mathrm{TE}^Y} = A \cdot \vec{E}_{\mathrm{TE}^Z} + B \cdot \vec{E}_{\mathrm{TM}^Z}. \tag{1}$$

The explicit field components for the electric fields in (1), expressed with the hybrid TE_1^Y modal functions [10] and with the nonhybrid TE_1^Z and TM_1^Z modal functions [14], are given in the Appendix . Equating the progressive-wave terms (e^{-jkzz})

of (1), the coefficients A and B are readily obtained as follows (where the definition of N, k_x, and k_y can be found in the Appendix):

$$A = \frac{-k_y \cdot N}{{k_x}^2 + {k_y}^2} \quad B = \frac{jk_x \cdot N}{{k_x}^2 + {k_y}^2}. \tag{2}$$

With these projection coefficients (A and B), and equating the regressive-wave terms (e^{+jkzz}) in (1), the following equations are obtained to relate the TE_1^Y hybrid reflection coefficient R^{TE} to the nonhybrid TE_1^Z and TM_1^Z reflection and coupling coefficients (ρ^{TE}, ρ^{TM}, τ^{TE}, and τ^{TM}):

$$+jR^{\mathrm{TE}} = \frac{+jk_y{}^2}{{k_x}^2 + {k_y}^2}\rho^{\mathrm{TE}} + \frac{-jk_y \cdot k_x}{{k_x}^2 + {k_y}^2}\tau^{\mathrm{TE}} + \frac{+jk_x{}^2}{{k_x}^2 + {k_y}^2}\rho^{\mathrm{TM}} + \frac{k_y \cdot k_x}{{k_x}^2 + {k_y}^2}\tau^{\mathrm{TM}} \tag{3}$$

$$0 = k_y \cdot k_x \cdot \left(\rho^{\mathrm{TM}} - \rho^{\mathrm{TE}}\right) + jk_x{}^2 \cdot \tau^{\mathrm{TE}} - jk_y{}^2 \cdot \tau^{\mathrm{TM}}. \tag{4}$$

In the same manner, one can study the scenario in which a TM_1^Y wave is incident at a radiating open end, also represented in Fig. 3. In this case, it is more convenient to express the total magnetic field associated to the TM_1^Y parallel-plate mode, and project it as a sum of a TE_1^Z wave and a TM_1^Z wave, each one with a given complex factor (C and D, respectively)

$$\vec{H} = \vec{H}_{\mathrm{TM}^Y} = C \cdot \vec{H}_{\mathrm{TE}^Z} + D \cdot \vec{H}_{\mathrm{TM}^Z}. \tag{5}$$

The explicit field components for the magnetic fields in (5) are given in the Appendix for both the hybrid TM_1^Y mode [10] and also for the nonhybrid TE_1^Z and TM_1^Z modal functions [14]. Equating the progressive-wave terms (e^{-jkzz}) of (5), the coefficients C and D are obtained as follows:

$$C = \frac{-\omega\varepsilon \cdot k_x \cdot k_z \cdot N}{\left(k_0{}^2 - k_y{}^2\right) \cdot \left(k_x{}^2 + k_y{}^2\right)}$$
$$D = \frac{-j\omega\varepsilon \cdot k_x \cdot k_z \cdot k_y}{\left(k_0{}^2 - k_y{}^2\right) \cdot \left(k_x{}^2 + k_y{}^2\right)}. \tag{6}$$

Using the coefficients C and D expressed in (6), the regressive-wave terms (e^{+jkzz}) of (5) can be compared, obtaining the following equations to relate the TM_1^Y hybrid reflection coefficient (R^{TM}) to the TE_1^Z and TM_1^Z reflection and coupling coefficients (ρ^{TE}, ρ^{TM}, τ^{TE}, and τ^{TM}):

$$R^{\mathrm{TM}} = \frac{k_x{}^2}{{k_x}^2 + {k_y}^2}\rho^{\mathrm{TE}} + \frac{-jk_yk_x}{{k_x}^2 + {k_y}^2}\tau^{\mathrm{TE}} + \frac{k_y{}^2}{{k_x}^2 + {k_y}^2}\rho^{\mathrm{TM}} + \frac{jk_yk_x}{{k_x}^2 + {k_y}^2}\tau^{\mathrm{TM}} \tag{7}$$

$$0 = jk_y \cdot k_x \left(\rho^{\mathrm{TE}} - \rho^{\mathrm{TM}}\right) + k_x{}^2 \cdot \tau^{\mathrm{TE}} - k_y{}^2 \cdot \tau^{\mathrm{TM}}. \tag{8}$$

Using (3), (4), (7), and (8), the following relations are obtained for the nonhybrid TE_1^Z and TM_1^Z reflection and coupling coefficients:

$$\rho^{\mathrm{TE}} = \left(k_x{}^2 + k_y{}^2\right) \cdot \chi \cdot \left[\frac{R^{\mathrm{TE}}}{k_x{}^2} - \frac{R^{\mathrm{TM}}}{k_y{}^2}\right] \tag{9}$$

$$\rho^{\mathrm{TM}} = \left(k_x{}^2 + k_y{}^2\right) \cdot \chi \cdot \left[\frac{R^{\mathrm{TM}}}{k_x{}^2} - \frac{R^{\mathrm{TE}}}{k_y{}^2}\right] \tag{10}$$

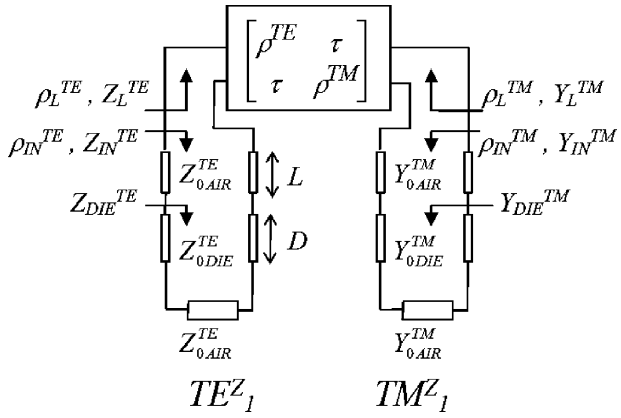

Fig. 4. Impedances and reflection coefficients used in the description of the nonhybrid equivalent transverse network.

$$\tau = \tau^{\mathrm{TE}} = \tau^{\mathrm{TM}} = j \cdot \left(k_x{}^2 + k_y{}^2\right) \cdot \chi \cdot \left[\frac{R^{\mathrm{TM}} - R^{\mathrm{TE}}}{k_x \cdot k_y}\right] \tag{11}$$

$$\chi = \frac{k_x{}^2 \cdot k_y{}^2}{k_x{}^4 - k_y{}^4}. \tag{12}$$

Equations (9)–(12) allow to relate the reflections and coupling coefficients (ρ^{TE}, ρ^{TM}, and τ) of the novel nonhybrid model (TE_1^Z and TM_1^Z) with the reflection coefficients (R^{TE} and R^{TM}) of the hybrid model (TE_1^Y and TM_1^Y) developed in [10].

Once the nonhybrid coefficients have been expressed in (9)–(12), the top radiating aperture can be described to obtain the novel transverse equivalent network for the nonhybrid TE_1^Z and TM_1^Z modes. This transverse equivalent network was shown in Fig. 2(b), and it is illustrated with more detail in Fig. 4. As can be seen in Fig. 4, an original two-port circuit interconnects the TE_1^Z transverse equivalent circuit to the TM_1^Z transverse equivalent circuit, modeling the top radiating impedance seen by this set of coupled nonhybrid modes. The two-port interconnecting circuit can be described with its corresponding S-parameter matrix [17], which allows to take into account for the reflection created at the radiating discontinuity (modeled by the reflections coefficients ρ^{TE} and ρ^{TM}), and also for the coupling between the TE_1^Z and TM_1^Z modes (modeled by the coupling coefficient τ)

$$S = \begin{bmatrix} \rho^{\mathrm{TE}} & \tau \\ \tau & \rho^{\mathrm{TM}} \end{bmatrix}. \tag{13}$$

The equivalent reflection coefficients seen by each TE_1^Z and TM_1^Z mode at the radiating discontinuity (ρ_L^{TE} and ρ_L^{TM}, illustrated in Fig. 4) can be computed using the S-parameters (13), obtaining the following expressions:

$$\rho_L^{\mathrm{TE}} = \rho^{\mathrm{TE}} + \tau^2 \frac{\rho_{\mathrm{IN}}^{\mathrm{TM}}}{1 - \rho^{\mathrm{TM}} \cdot \rho_{\mathrm{IN}}^{\mathrm{TM}}} \tag{14}$$

$$\rho_L^{\mathrm{TM}} = \rho^{\mathrm{TM}} + \tau^2 \frac{\rho_{\mathrm{IN}}^{\mathrm{TE}}}{1 - \rho^{\mathrm{TE}} \cdot \rho_{\mathrm{IN}}^{\mathrm{TE}}}. \tag{15}$$

As can be easily seen by inspecting (14) and (15), the nonhybrid TE_1^Z and TM_1^Z transverse equivalent networks shown in Fig. 4 are coupled due to the coupling coefficient τ. In (14)

and (15), $\rho_{\rm IN}^{\rm TE}$ and $\rho_{\rm IN}^{\rm TM}$ are the modal reflections coefficients seen from the top of each equivalent transmission circuit to the bottom (see Fig. 4). They can be computed using basic formulas for transmission lines [17]. The equivalent radiating aperture impedances ($Z_L^{\rm TE}$ and $Y_L^{\rm TM}$, in Fig. 4) can be computed from $\rho_L^{\rm TE}$ and $\rho_L^{\rm TM}$ in the following way:

$$Z_L^{\rm TE} = Z_0^{\rm TE}\frac{1+\rho_L^{\rm TE}}{1-\rho_L^{\rm TE}} \quad Y_L^{TM} = Y_0^{\rm TM}\frac{1-\rho_L^{\rm TM}}{1+\rho_L^{\rm TM}} \qquad (16)$$

where $Z_0^{\rm TE}$ and $Y_0^{\rm TM}$ are the characteristic impedances of the $\rm TE_1^Z$ and $\rm TM_1^Z$ modes [14]. The rest of the impedances and admittances needed to describe the nonhybrid transverse circuit illustrated in Fig. 4 can be computed in a similar way using basic transmission line equations [17].

III. Results

To validate the new equivalent circuit developed in this paper, the NRD leaky-wave antenna presented in [9]–[11] is going to be studied. This structure was analyzed using an equivalent transverse network entirely developed for hybrid $\rm TE_1^Y$ and $\rm TM_1^Y$ modes, which was illustrated in Fig. 2(a). We will now study the same structure using the new equivalent network shown in Figs. 2(b) and 4. As it can be seen from Fig. 2, the hybrid model [see Fig. 2(a)] is much more complicated than the nonhybrid equivalent circuit [see Fig. 2(b)] due to the fact that the coupling between hybrid modes is created in the air–dielectric interface in the form of a shunt transformer. This makes it necessary to study the circuit via a hybrid method, combining nodal and mesh equations, which complicate the transverse resonance equation, as described in detail in [10]. On the contrary, the nonhybrid model [see Fig. 2(b)] makes use of a simple coupling network, which is characterized by its four S-parameters (13). In this way, all the impedances are shunt cascaded with the nonhybrid model, as can be seen in Fig. 4. The transverse resonance equation of this coupled transmission-lines model can be easily described by the following equations, which depend on the unknown longitudinal propagation constant k_y

$$Z_{\rm IN}^{\rm TE}(k_y) + Z_L^{\rm TE}(k_y) = 0 \rightarrow F^{\rm TE}(k_y) = 0 \qquad (17)$$
$$Y_{\rm IN}^{\rm TM}(k_y) + Y_L^{\rm TM}(k_y) = 0 \rightarrow F^{\rm TM}(k_y) = 0. \qquad (18)$$

The impedances and admittances used in (17) and (18) are illustrated in Fig. 4, and all of them can be analytically expressed in closed form. $Z_L^{\rm TE}$ and $Y_L^{\rm TM}$ are described in (14)–(16), and $Z_{\rm IN}^{\rm TE}$ and $Y_{\rm IN}^{\rm TM}$ can be analytically expressed using basic transmission line equations [17]. The zeros of (17) and (18) must be numerically found, each one corresponding to a propagation mode of the studied NRD guide. In the case of a leaky-wave mode, its propagation constant is complex due to radiation losses ($k_y = \beta - j\alpha$), and the numerical search must be performed in the complex plane, as was done in [14].

The following results describe different dispersion curves obtained for the main mode of an NRD guide. This mode corresponds to the first zero of the $\rm TM^Z$ transverse resonance (18). The dimensions of the stub-shortened NRD leaky-wave antenna according to the inset of Fig. 5 are $a = 2.7$ mm, $D = 2.4$ mm, $\varepsilon_r = 2.56$, and $L = 2.8$ mm, and the frequency of analysis is

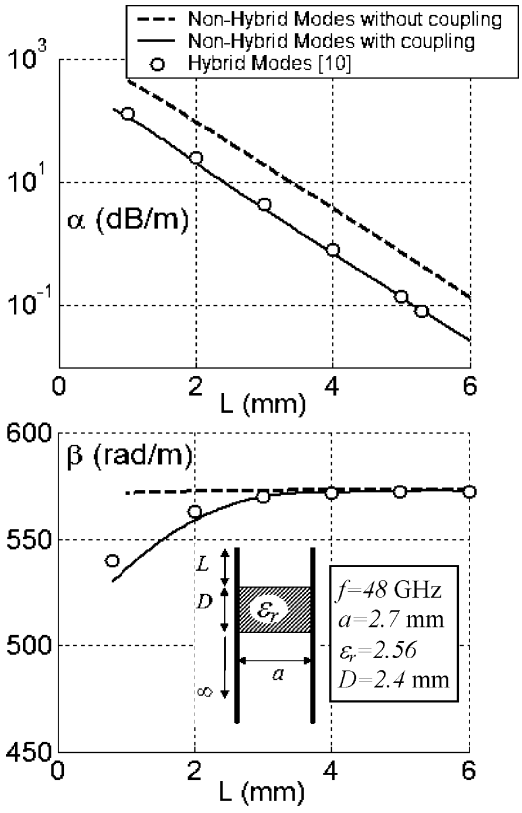

Fig. 5. Leakage and phase constant as a function of the stub-height L.

$f = 48$ GHz. Fig. 5 shows the variation of the phase and leakage constants as a function of the stub height L. Three different curves are plotted in Fig. 5. The results obtained in [10] using the hybrid modes equivalent network [see Fig. 2(a)] are plotted with circles to validate our results. The results obtained with the new nonhybrid model are plotted via a continuous line, observing excellent agreement for both the leakage rate and phase constant. In this figure, also illustrated is the necessity to take into account the coupling coefficient between the $\rm TE_1^Z$ and $\rm TM_1^Z$ transmission lines [τ, (11) and (12)]. For this purpose, τ was neglected in our model to obtain the results plotted via a dashed line in Fig. 5. As can be seen, the results obtained are wrong, presenting a higher leakage rate for all values of L, and a strong deviation for the phase constant below $L = 3$ mm. Therefore, the coupling between $\rm TE_1^Z$ and $\rm TM_1^Z$ modes due to the radiating aperture must be considered to obtain accurate results.

Fig. 6 shows the dispersion curves for the same NRD leaky-wave antenna, but now modifying the dielectric guide width a. Again, very good agreement is observed between the hybrid model and nonhybrid model, validating the new transverse equivalent network.

Finally, Figs. 7 and 8 show other dispersion curves obtained in [10], this time varying the height D of the NRD guide, and its dielectric permittivity ε_r. In both cases, excellent agreement is obtained for both the phase and attenuation constants, even in the cutoff regime (for very low values of β, $\beta/k_0 < 0.2$), where α becomes very large due to reactive attenuation of the leaky mode. As has been illustrated, the accuracy of the proposed equivalent network is the same as the one proposed in [10], but it provides simpler dispersion equations. This simplification is

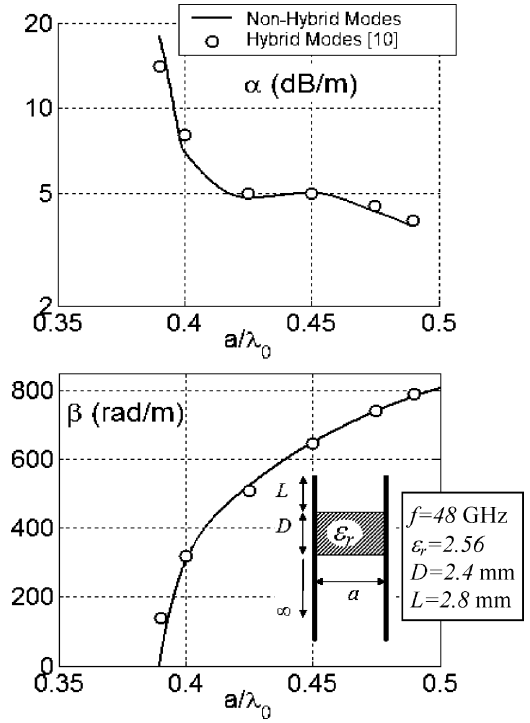

Fig. 6. Leakage and phase constant as a function of the dielectric guide width a.

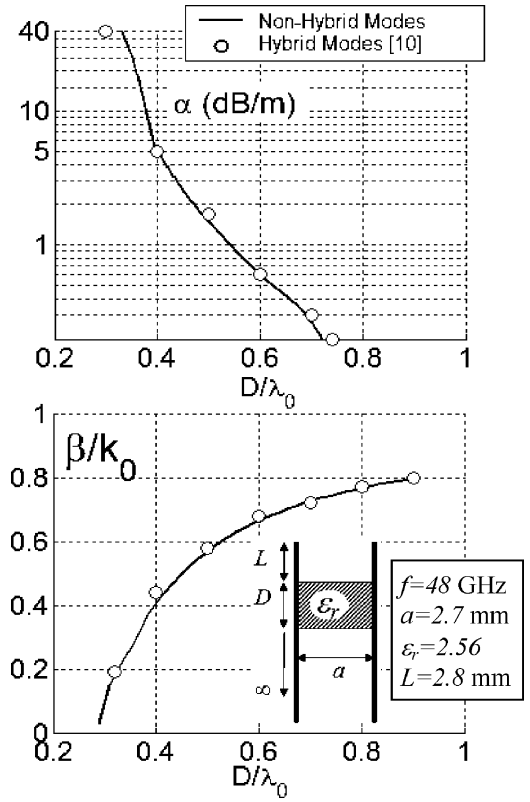

Fig. 7. Leakage and phase constant as a function of the dielectric guide height D.

more evident when one wants to introduce these equivalent networks in the associated parallel-plate Green's functions, for instance, to study lines or slots printed at the air–dielectric interface of the NRD guide [14], [15].

Another application of the theory presented is the investigation of cross-polarization components in the leaky-wave an-

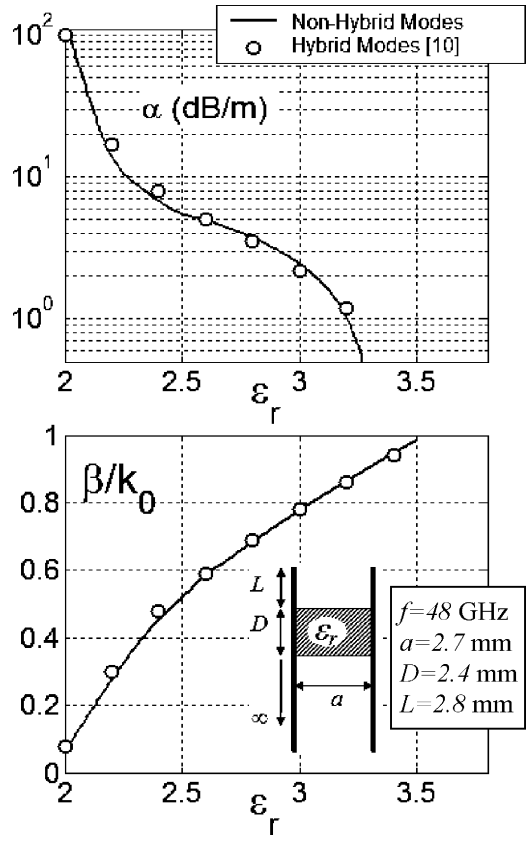

Fig. 8. Leakage and phase constant as a function of the dielectric constant ε_r.

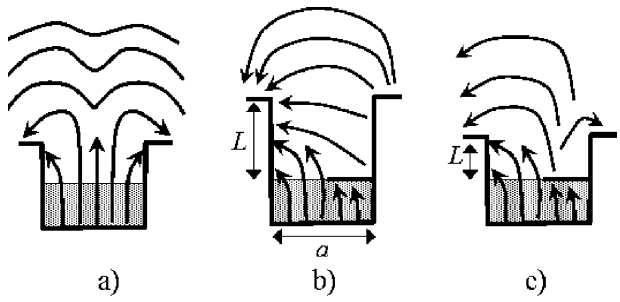

Fig. 9. Scenarios that illustrate the necessity to consider the radiation from main and first higher order parallel-plate mode at the same time.

tennas shown in Fig. 9. Fig. 9(a) presents the conventional stub-shortened leaky-wave antenna, showing the vertical component of the radiating fields associated to the first higher order parallel-plate mode. This structure can be complicated by adding an asymmetric slot in the dielectric interface [16], as is shown in Fig. 9(b). In this case, the vertical field of the dielectric guide is transformed into a horizontal radiating field, which corresponds to the main parallel-plate mode. As has been commented in Section I, one can only take into account the radiation of the main parallel-plate mode (neglecting the radiation from higher order parallel-plate modes) if the stub is high enough [1]–[7], [14]–[16]. However, the stub can be shortened to obtain a vertical component of the radiated fields, which is added to the horizontal component in order to synthesize any type of polarization in the far field, as described in detail in [18] and [19]. This situation is illustrated in Fig. 9(c). For this case, one has to study at the same time the radiation of the main parallel-plate mode and

the two first higher order parallel-plate modes. For this study, it is very convenient to use the new transverse equivalent network, and introduce it in the constituent Green's functions of the problem [14], [15]. Therefore, the alternative equivalent network developed in this study can simplify the study of many structures due to the use of nonhybrid parallel-plate modes.

IV. Conclusion

An original equivalent network has been developed to accurately model the radiation from higher order parallel-plates modes below cutoff. The new transverse circuit is based on the expansion of the nonhybrid modes of the parallel plates. In this way, the interfaces between different materials can simply be characterized using cascaded equivalent transmission lines. The radiating open end of the parallel plates makes the nonhybrid modes to couple. An equivalent two-port circuit has been developed to take into account both the radiation and the coupling that occurs in the radiating discontinuity. The new model has been validated by obtaining leaky-mode dispersion curves for a leaky-wave antenna in NRD guide technology. Results are compared to those obtained using hybrid modes, showing excellent agreement. The proposed equivalent network allows to obtain simpler transverse resonance equations than using hybrid modes, while keeping the same accuracy.

Appendix
Vector Modal Fields for Hybrid and Nonhybrid TE_1 and TM_1 Parallel-Plate Modes in the Presence of Radiating Open End

The mode functions presented here are those appropriate to the scenarios illustrated in Fig. 3. For the case in which a hybrid TE_1^Y mode is incident in the parallel-plate radiating open end, the top radiating open end can be modeled by a simple equivalent reflection coefficient R^{TE} [10]. The total electric field in the parallel-plate region, taking into account the incident and the reflected wave, can be expressed as [10]

$$\begin{aligned}\vec{E} &= \vec{E}_{\mathrm{TE}^Y} \\ &= -j\sqrt{\frac{2}{a}}\left(e^{-jk_z z} + R^{\mathrm{TE}} e^{+jk_z z}\right) \\ &\quad \cdot \cos(k_x \cdot x) \cdot e^{-jk_y y} \cdot \hat{x} \\ &\quad + \frac{-jk_x}{k_z}\sqrt{\frac{2}{a}}\left(e^{-jk_z z} - R^{\mathrm{TE}} e^{+jk_z z}\right) \\ &\quad \cdot \sin(k_x \cdot x) \cdot e^{-jk_y y} \cdot \hat{z} \end{aligned} \tag{A1}$$

where $k_x = \pi/a$, k_y is the unknown longitudinal propagation constant, and k_z is the transverse propagation constant, which are related by the following equation (where k_0 is the free-space wavenumber):

$$k_0{}^2 = k_x{}^2 + k_y{}^2 + k_z{}^2. \tag{A2}$$

On the other hand, the total electric field in the scenario of Fig. 3 can also be expressed as a sum of a TE_1^Z wave and a TM_1^Z wave (nonhybrid modes, [14]), each one with a given complex factor [A and B, respectively, following the same notation as in (1)]. The equivalent reflection coefficients (ρ^{TE} and ρ^{TM}) and the coupling coefficients (τ^{TE} and τ^{TM}) shown in Fig. 3 must be considered for the expansion of the fields using the nonhybrid set of modes TE_1^Z and TM_1^Z, obtaining the following results:

$$\begin{aligned}\vec{E} &= A \cdot \vec{E}_{\mathrm{TE}^Z} + B \cdot \vec{E}_{\mathrm{TM}^Z} \\ &= A \cdot \left\{ \frac{-jk_y}{N}\sqrt{\frac{2}{a}}\left(e^{-jk_z z} + \rho^{\mathrm{TE}} e^{+jk_z z}\right) \right. \\ &\qquad \left. + \tau^{\mathrm{TE}} \frac{+k_x}{N}\sqrt{\frac{2}{a}} \cdot e^{+jk_z z} \right\} \cdot \cos(k_x x) \cdot e^{-jk_y y} \cdot \hat{x} \\ &\quad + B \cdot \left\{ \frac{+k_x}{N}\sqrt{\frac{2}{a}}\left(e^{-jk_z z} + \rho^{\mathrm{TM}} e^{+jk_z z}\right) \right. \\ &\qquad \left. + \tau^{\mathrm{TM}} \frac{-jk_y}{N}\sqrt{\frac{2}{a}} \cdot e^{+jk_z z} \right\} \\ &\quad \cdot \cos(k_x x) \cdot e^{-jk_y y} \cdot \hat{x} \\ &\quad + A \cdot \left\{ \frac{+k_x}{N}\sqrt{\frac{2}{a}}\left(e^{-jk_z z} + \rho^{\mathrm{TE}} e^{+jk_z z}\right) \right. \\ &\qquad \left. + \tau^{\mathrm{TE}} \frac{-jk_y}{N}\sqrt{\frac{2}{a}} \cdot e^{+jk_z z} \right\} \\ &\quad \cdot \sin(k_x x) \cdot e^{-jk_y y} \cdot \hat{y} \\ &\quad + B \cdot \left\{ \frac{-jk_y}{N}\sqrt{\frac{2}{a}}\left(e^{-jk_z z} + \rho^{\mathrm{TM}} e^{+jk_z z}\right) \right. \\ &\qquad \left. + \tau^{\mathrm{TM}} \frac{+k_x}{N}\sqrt{\frac{2}{a}} \cdot e^{+jk_z z} \right\} \\ &\quad \cdot \sin(k_x x) \cdot e^{-jk_y y} \cdot \hat{y} \\ &\quad + A \cdot \left\{ (-\tau^{\mathrm{TE}}) \left(-\frac{k_x{}^2 + k_y{}^2}{jk_z N}\right) \sqrt{\frac{2}{a}} \cdot e^{+jk_z z} \right\} \\ &\quad \cdot \sin(k_x x) \cdot e^{-jk_y y} \cdot \hat{z} \\ &\quad + B \cdot \left\{ \left(-\frac{k_x{}^2 + k_y{}^2}{jk_z N}\right) \sqrt{\frac{2}{a}} \cdot \left(e^{-jk_z z} - \rho^{\mathrm{TM}} e^{+jk_z z}\right) \right\} \\ &\quad \cdot \sin(k_x x) \cdot e^{-jk_y y} \cdot \hat{z}. \end{aligned} \tag{A3}$$

where the normalization factor N is defined as [14]

$$N = \sqrt{k_x{}^2 + |k_y|^2}. \tag{A4}$$

The second case represented in Fig. 3 is that of a hybrid TM_1^Y mode, which is incident in the parallel-plate radiating open end, now modeled by the equivalent reflection coefficient R^{TM} [10]. In this case, it is more convenient to express the magnetic field associated to the hybrid TM_1^Y parallel-plate mode [10]

$$\begin{aligned}\vec{H} &= \vec{H}_{\mathrm{TE}^Y} \\ &= \frac{k_z \omega \varepsilon}{k_0{}^2 - k_y{}^2}\sqrt{\frac{2}{a}}\left(e^{-jk_z z} - R^{\mathrm{TM}} e^{+jk_z z}\right) \\ &\quad \cdot \sin(k_x x) \cdot e^{-jk_y y} \cdot \hat{x} \\ &\quad + \frac{-j\omega\varepsilon \cdot k_x}{k_0{}^2 - k_y{}^2}\sqrt{\frac{2}{a}}\left(e^{-jk_z z} - R^{\mathrm{TM}} e^{+jk_z z}\right) \\ &\quad \cdot \cos(k_x x) \cdot e^{-jk_y y} \cdot \hat{z}. \end{aligned} \tag{A5}$$

As was done for the TE_1^Y field, the TM_1^Y magnetic field can be projected as a sum of a TE_1^Z wave and a TM_1^Z wave, each one

with a given complex factor [C and D respectively, following the same notation as in (5)]. Using the vector modal magnetic functions for the nonhybrid modes [14], and taking into account the reflection coefficients (ρ^{TE} and ρ^{TM}) and the coupling coefficients (τ^{TE} and τ^{TM}) shown in Fig. 3, the following expression can be obtained:

$$
\begin{aligned}
\vec{H} =& C \cdot \vec{H}_{\mathrm{TE}^z} + D \cdot \vec{H}_{\mathrm{TM}^z} \\
=& C \cdot \left\{ \frac{-k_x}{N}\sqrt{\frac{2}{a}}\left(e^{-jk_z z} - \rho^{\mathrm{TE}} e^{+jk_z z}\right) \right. \\
& \left. - \tau^{\mathrm{TE}} \frac{+jk_y}{N}\sqrt{\frac{2}{a}} \cdot e^{+jk_z z} \right\} \\
& \cdot \sin(k_x x) \cdot e^{-jk_y y} \cdot \hat{x} \\
& + D \cdot \left\{ \frac{+jk_y}{N}\sqrt{\frac{2}{a}}\left(e^{-jk_z z} - \rho^{\mathrm{TM}} e^{+jk_z z}\right) \right. \\
& \left. - \tau^{\mathrm{TM}} \frac{-k_x}{N}\sqrt{\frac{2}{a}} \cdot e^{+jk_z z} \right\} \\
& \cdot \sin(k_x x) \cdot e^{-jk_y y} \cdot \hat{x} \\
& + C \cdot \left\{ \frac{-jk_y}{N}\sqrt{\frac{2}{a}}\left(e^{-jk_z z} - \rho^{\mathrm{TE}} e^{+jk_z z}\right) \right. \\
& \left. - \tau^{\mathrm{TE}} \frac{+k_x}{N}\sqrt{\frac{2}{a}} \cdot e^{+jk_z z} \right\} \\
& \cdot \cos(k_x x) \cdot e^{-jk_y y} \cdot \hat{y} \\
& + D \cdot \left\{ \frac{+k_x}{N}\sqrt{\frac{2}{a}}\left(e^{-jk_z z} - \rho^{\mathrm{TM}} e^{+jk_z z}\right) \right. \\
& \left. - \tau^{\mathrm{TM}} \frac{-jk_y}{N}\sqrt{\frac{2}{a}} \cdot e^{+jk_z z} \right\} \\
& \cdot \cos(k_x x) \cdot e^{-jk_y y} \cdot \hat{y} \\
& + C \cdot \left\{ \left(-\frac{{k_x}^2 + {k_y}^2}{jk_z N}\right)\sqrt{\frac{2}{a}} \cdot \left(e^{-jk_z z} + \rho^{\mathrm{TE}} e^{+jk_z z}\right) \right\} \\
& \cdot \cos(k_x x) \cdot e^{-jk_y y} \cdot \hat{z} + \\
& + D \cdot \left\{ \left(+\tau^{\mathrm{TM}}\right)\left(-\frac{{k_x}^2 + {k_y}^2}{jk_z N}\right)\sqrt{\frac{2}{a}} \cdot e^{+jk_z z} \right\} \\
& \cdot \cos(k_x x) \cdot e^{-jk_y y} \cdot \hat{z}. \qquad \text{(A6)}
\end{aligned}
$$

ACKNOWLEDGMENT

The authors gratefully acknowledge the helpful discussions maintained with Dr. D. Jackson, University of Houston, Houston, TX.

REFERENCES

[1] P. Lampariello and A. A. Oliner, "A new leaky-wave antenna for millimeter waves using an asymmetric strip in groove guide. Part I: Theory," *IEEE Trans. Antennas Propag.*, vol. AP-33, no. 12, pp. 1285–1294, Dec. 1985.

[2] Z. Ma and E. Yamashita, "Leakage characteristics of groove guide having a conductor strip," *IEEE Trans. Microw. Theory Tech.*, vol. 42, no. 10, pp. 1925–1931, Oct. 1994.

[3] F. Frezza, M. Guglielmi, and P. Lampariello, "Millimeter wave leaky-wave antennas based on slitted asymmetric ridge waveguides," *Proc. Inst. Elect. Eng.—Antennas Propag.*, vol. 141, pt. H, pp. 175–180, Jun. 1994.

[4] P. Lampariello, F. Frezza, H. Shigesawa, M. Tsuji, and A. A. Oliner, "A versatile leaky-wave antenna based on stub-loaded rectangular waveguide. Part I: Theory," *IEEE Trans. Antennas Propag.*, vol. 46, no. 7, pp. 1032–1041, Jul. 1998.

[5] H. Shigesawa, M. Tsuji, and A. A. Oliner, "Effects of air gap and finite metal plate width on NRD guide," in *IEEE MTT-S Int. Microw. Symp. Dig.*, Baltimore, MD, Jun. 1986, pp. 119–122.

[6] Z. Ma and E. Yamashita, "Leakage characteristics of groove guide having a conductor strip," *IEEE Trans. Microw. Theory Tech.*, vol. 42, no. 10, pp. 1925–1931, Oct. 1994.

[7] S. J. Xu, X.-Y. Zeng, K. Wu, and K.-M. Luk, "Characteristics and design consideration of leaky-wave NRD-guides for use as millimeter wave antenna," *IEEE Trans. Microwave Theory Tech.*, vol. 46, no. 12, pp. 2450–2456, Dec. 1998.

[8] T. Yoneyama and S. Nishida, "Nonradiative dielectric waveguide for millimeter wave integrated circuits," *IEEE Trans. Microw. Theory Tech.*, vol. MTT-29, no. 11, pp. 1188–1192, Nov. 1981.

[9] A. Sanchez and A. A. Oliner, "Accurate theory for a new leaky-wave antenna for millimetre wave using nonradiative dielectric waveguide," *Radio Sci.*, vol. 19, no. 5, pp. 1225–1228, Sep. 1984.

[10] A. Sanchez and A. A. Oliner, "A new leaky waveguide for millimeter waves using nonradiative dielectric (NRD) waveguide—Part I: Accurate theory," *IEEE Trans. Microw. Theory Tech.*, vol. MTT-35, no. 8, pp. 737–747, Aug. 1987.

[11] A. Sanchez and A. A. Oliner, "A new leaky waveguide for millimeter waves using nonradiative dielectric (NRD) waveguide—Part II: Comparison with experiments," *IEEE Trans. Microw. Theory Tech.*, vol. MTT-35, no. 8, pp. 748–752, Aug. 1987.

[12] N. Marcuvitz, *Waveguide Handbook*. New York: McGraw-Hill, 1951, pp. 179–181.

[13] L. A. Weinstein, *The Theory of Diffraction and the Factorization Method* (in Russian). Boulder, CO: Golem, 1969, pp. 29–50.

[14] J. L. Gómez and A. A. Melcón, "Nonorthogonality relations between complex-hybrid-modes: An application for the leaky-wave analysis of laterally-shielded top-open planar transmission lines," *IEEE Trans. Microw. Theory Tech.*, vol. 52, no. 3, pp. 760–767, Mar. 2004.

[15] J. L. Gómez and A. A. Melcón, "Radiation analysis in the space domain of laterally-shielded planar transmission lines. Part I: Theory," *Radio Sci.*, vol. 39, no. RS3005, pp. 1–11, Jun. 2004.

[16] J. L. Gómez, A. de la Torre, D. Cañete, M. Gugliemi, and A. A. Melcón, "Design of tapered leaky-wave antennas in hybrid waveguide-planar technology for millimeter waveband applications," *IEEE Trans. Antennas Propag.*, vol. 53, no. 8, pp. 2563–2577, Aug. 2005.

[17] D. M. Pozar, *Microwave Engineering*, 3rd ed. New York: Wiley, 1998.

[18] J. L. Gomez, G. Goussetis, D. Canete, F. Quesada, and A. A. Melcón, "Novel and simple technique to control the polarization in stub-loaded leaky-wave antennas," in *IEEE AP-S Int. Symp. Dig.*, Honolulu, HI, Jun. 9–15, 2007, pp. 5801–5804.

[19] J. L. Gómez, G. Goussetis, and A. A. Melcón, "Simple control of the polarisation in uniform hybrid waveguide-planar leaky-wave antennas," *IET Microw., Antennas, Propag.*, vol. 1, no. 4, pp. 911–917, Aug. 2007.

José Luis Gómez-Tornero (M'06) was born in Murcia, Spain, in 1977. He received the Telecommunications Engineer degree from the Universidad Politécnica de Valencia (UPV), Valencia, Spain, in 2001, and the Ph.D. degree (*laurea cum laude*) in telecommunication engineering from the Technical University of Cartagena (UPCT), Cartagena, Spain, in 2005.

In 1999, he joined the Radiocommunications Department, UPV, as a Research Student, where he was involved in the development of analytical and numerical tools for the study and automated design of microwave filters in waveguide technology for space applications. In 2000, he joined the Radio Frequency Division, Industry Alcatel Espacio, Madrid, Spain, where he was involved with the development of microwave active circuits for telemetry, tracking, and control (TTC) transponders implicated in many different spatial missions for the European Space Agency (ESA), National Aeronautics Space Administration (NASA), and other space agencies. In 2001, he joined the UPCT, as an Assistant Professor, where he currently develops his teaching activities. Since October 2005, he has been Vice Dean for students and lecture affairs with the Telecommunication Engineering Faculty, UPCT. His scientific research is focused on the analysis and design of leaky-wave antennas for millimeter waveband applications and the development of numerical methods for the analysis of novel

passive radiating structures in planar and waveguide technologies. His scientific interests also include the study of active devices for microwave and millimeter wavebands such as oscillators and active antennas.

Dr. Gómez-Tornero was the recipient of the 2004 Second National Award presented by the EPSON-Ibérica Foundation for the best doctoral project in the field of technology of information and communications (TIC). He was also the recipient of the 2006 Vodafone Foundation Colegio Oficial de Ingenieros de Telecomunicación (COIT/AEIT) Award presented to the best Spanish doctoral thesis in the area of advanced mobile communications technologies.

Fernando Daniel Quesada-Pereira (S'05–M'07) was born in Murcia, Spain, in 1974. He received the Telecommunications Engineer degree from the Technical University of Valencia (UPV), Valencia, Spain, in 2000, and the Ph.D. degree from the Technical University of Cartagena (UPCT), Cartagena, Spain in 2007.

In 1999, he joined the Radiocommunications Department, UPV, as a Research Assistant, where he was involved in the development of numerical methods for the analysis of anechoic chambers and tag antennas. In 2001, he joined UPCT, initially as an Research Assistant, and then as an Assistant Professor. His current scientific interests include the integral-equation technique applied to the analysis of antennas and microwave devices.

Alejandro Álvarez-Melcón (M'99–SM'07) was born in Madrid, Spain, in 1965. He received the Telecommunications Engineer degree from the Technical University of Madrid (UPM), Madrid, Spain, in 1991, and the Ph.D. degree in electrical engineering from the Swiss Federal Institute of Technology, Lausanne, Switzerland, in 1998.

In 1988, he joined the Signal, Systems and Radiocommunications Department, UPM, as a Research Student, where he was involved in the design, testing, and measurement of broadband spiral antennas for electromagnetic measurements support (EMS) equipment. From 1991 to 1993, he was with the Radio Frequency Systems Division, European Space Agency (ESA)/European Space Research and Technology Centre (ESTEC), Noordwijk, The Netherlands, where he was involved in the development of analytical and numerical tools for the study of waveguide discontinuities, planar transmission lines, and microwave filters. From 1993 to 1995, he was with the Space Division, Industry Alcatel Espacio, Madrid, Spain, and also with the ESA, where he collaborated on several ESA/ESTEC contracts. From 1995 to 1999, he was with the Swiss Federal Institute of Technology, École Polytechnique Fédérale de Lausanne (EPFL), Lausanne, Switzerland, where he was involved in the field of microstrip antennas and printed circuits for space applications. In 2000, he joined the Technical University of Cartagena (UPCT), Cartagena, Spain, where he currently develops his teaching and research activities.

Dr. Alvarez-Melcón was the recipient of the *Journée Internationales de Nice Sur les Antennes* (JINA) Best Paper Award for the best contribution to the JINA'98 International Symposium on Antennas, and the Colegio Oficial de Ingenieros de Telecomunicación (COIT/AEIT) Award for the best doctoral thesis in basic information and communication technologies.